

A polynomial time algorithm for studying physical observables in chaotic eigenstates

Pavan Hosur

*Department of Physics, University of Houston, Houston, TX 77204 and
Texas Center for Superconductivity, Houston, TX 77204*

(Dated: June 1, 2021)

We introduce an algorithm, the Orthogonal Operator Polynomial Expansion (OOPEX), to approximately compute expectation values in energy eigenstates at finite energy density of non-integrable quantum many-body systems with polynomial effort, whereas exact diagonalization (ED) of the Hamiltonian H is exponentially hard. The OOPEX relies on the eigenstate thermalization hypothesis, which conjectures that eigenstate expectation values of physical observables in such systems vary smoothly with the eigenstate energy (and other macroscopic conserved quantities, if any), and computes them through a series generated by repeated multiplications, rather than diagonalization, of H and whose successive terms oscillate faster with the energy. The hypothesis guarantees that only the first few terms of this series contribute appreciably. We further show that the OOPEX, in a sense, is the most optimum algorithm based on series expansions of H as it avoids computing the many-body density of states which plagues other similar algorithms. Then, we argue non-rigorously that working in the Fock space of operators, rather than that of states as is usually done, yields convergent results with computational resources that scale polynomially with N . We demonstrate the polynomial scaling by applying the OOPEX to the non-integrable Ising chain and comparing with ED and high-temperature expansion (HTX) results. The OOPEX provides access to much larger N than ED and HTX do, which facilitates overcoming finite-size effects that plague the other methods to extract correlation lengths in chaotic eigenstates. In addition, access to large systems allows testing a recent conjecture that the Renyi entropy of chaotic eigenstates has positive curvature if the Renyi index > 1 , and we find encouraging supporting evidence.

I. INTRODUCTION

Some quantum many-body systems are integrable, i.e., they contain simplifying properties such as easy-to-diagonalize conserved operators, emergent conservation laws resulting from strong disorder [1–4] or factorizable scattering matrices [5–8] that make them computationally – and sometimes analytically – tractable. Most lack these properties and are said to be non-integrable (NI). Recent years have revealed that energy eigenstates with finite energy density in NI quantum many-body systems provide portals into diverse areas of physics and related fields. For instance, their properties relevant to condensed matter, quantum information, fundamental physics, gravity and statistical mechanics, respectively, include the facts that they encode finite temperature phase transitions [9, 10], form a quantum error correcting code [11–14], enable reconstruction of the entire Hamiltonian [15, 16], mimic conformal field theories [17–20] which in turn mimic quantum gravity under the holographic mapping [21, 22] and resemble equilibrium statistical ensembles if only simple measurements are made [23–32], where “simple” usually means few-body and local, and includes observables that real experiments can measure. Such eigenstates are also relevant to chaos, which earns then the name chaotic eigenstates. Firstly, if a quantum system has a well-defined classical limit and the classical system is chaotic, the quantum eigenstates are expected to satisfy the eigenstate thermalization hypothesis (ETH) [33–35]. Secondly, quantum systems with ETH-satisfying eigenstates exhibit, in many cases, temporal correlations that resemble the famous “butterfly effect” from classical chaos [30, 36–44]. These unique properties make simu-

lating chaotic eigenstates an important goal of quantum many-body physics.

Unfortunately, this is a Herculean task. Chaotic eigenstates occur at finite energy density above the ground state, which puts them beyond the reach of the numerous powerful algorithms available for studying ground state and low-energy physics. Quantum Monte Carlo methods *can* study physics at finite energy density with polynomial effort in N , the number of degrees of freedom, if a suitable discrete symmetry cures the sign-problem [45, 46]. If there is no symmetry – in which case the model is maximally NI – the sign-problem persists and the complexity becomes exponential. Finally, the lack of simplifying properties in NI systems makes brute force exact diagonalization (ED) of H exponentially hard. Thus, the problem of simulating chaotic eigenstates is generally deemed unsolvable.

In this work, we introduce an algorithm – the Orthogonal Operator Polynomial Expansion (OOPEX) – that extracts useful information from chaotic eigenstates with polynomial effort. It achieves this efficiency by exploiting the ETH, which states that $\langle A(E_i) \rangle$, the expectation value of any simple operator A in an energy eigenstate $|E_i\rangle$ of a NI Hamiltonian H , acquires the same value in nearby eigenstates at finite energy density in the thermodynamic limit:

$$\langle A(E_i) \rangle \xrightarrow{N \rightarrow \infty} \langle A(E_j) \rangle \text{ if } \frac{E_i - E_0}{N} \xrightarrow{N \rightarrow \infty} \frac{E_j - E_0}{N} \neq 0 \quad (1)$$

where E_0 is the ground state energy [15, 25, 32, 35]. For systems with a bounded spectrum such as lattice models, (1) is expected when E_0 refers to the highest energy state as well. Specifically, we will express $\rho(E_i) = |E_i\rangle\langle E_i|$

as a power series in H , modified such that higher order terms capture progressively more complicated observables. As a result, truncating the series retains only the simple, ETH-satisfying, experimentally accessible observables. In contrast, ED computes the full wavefunction exactly before extracting simple observables from it. This unnecessary computation is the source of ED's inefficiency. ED also requires storing H as a matrix in the local Fock basis, which consumes an exponential amount of memory. Here, we use the Operator Fock Space Representation (OFSR) [47, 48], which eliminates the need to store and manipulate state-vectors or operator-matrices and consequently reduces computational needs to merely polynomial in N . Crucially, we show that the OFSR is the natural language for developing the OOPEX.

The OOPEX is distinct from a simple high-temperature expansion (HTX), which entails Taylor expanding $e^{-\beta H}$ in powers of β but fails to exploit non-integrability of the system. As explained in Sec. II C, it also differs crucially from other polynomial expansion methods by avoiding computing the density of states $D(E)$. $D(E)$ is usually not well-approximated by polynomials, but algorithms such as the kernel polynomial method Weiße *et al.* [49] find a polynomial approximant to it nonetheless and thereby converge much slower.

II. THE ALGORITHM

A. ETH-based truncation

Suppose our goal is to compute $\langle A(E_i) \rangle = \text{tr}[\rho(E_i)A]$. If the spectrum of H lacks degeneracies, as is expected for NI systems, the Krylov space defined by $1, H, H^2 \dots H^{d-1}$, where d is the total Hilbert space dimension, forms a complete basis for the space of operators that commute with H . An alternate basis for this space is simply $\rho(E_i), i = 1 \dots d$. Therefore, $\rho(E_i)$ is expressible as a power series in H . A simple power series, however, does not produce progressively diminishing contributions to $\langle A(E_i) \rangle$, so its truncation error is uncontrolled. To rectify this problem, we first orthonormalize the Krylov space and write

$$\rho(E_i) = \sum_{m=0}^{d-1} p_m(E_i) p_m(H) \quad (2)$$

where $p_m(x) = \sum_{k=0}^m a_{km} x^k$ is an m^{th} degree polynomial of its argument that satisfies the orthogonality conditions: $\text{tr}[p_m(H)p_{m'}(H)] = \delta_{mm'}$, $\sum_{m=0}^{d-1} p_m(E_i)p_m(E_j) = \delta_{ij}$. Intuitively, i and m are conjugate variables with respect to the definition (2), analogous to the conjugacies of frequency and time with respect to Fourier transformation. While exact, (2) is impractical because d grows exponentially with N . We now argue, and later demonstrate using the NI Ising model, that $O(1)$ terms suffice in practice. Then, (2) involves

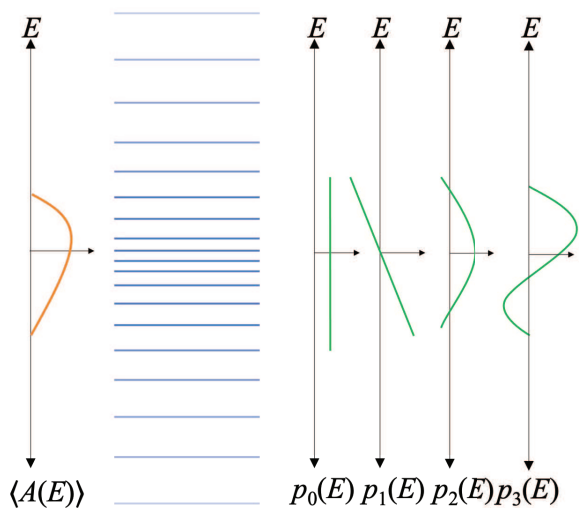


Figure 1. Schematic of the OOPEX philosophy. $\langle A(E) \rangle$ varies slowly with E far from the edges of the spectrum if A satisfies the ETH. $p_m(E)$ are polynomials with m roots, so they oscillate faster with E as m increases. Thus, according to (2), $\langle A(E) \rangle$ receives dominant contributions from small m .

computing only the first few powers of H via multiplication, which is far more efficient than diagonalizing it.

To see why only the first few terms suffice, recall that $p_m(E_i)$ is a polynomial in E_i of degree m , so it varies slowly (rapidly) with E_i for small (large) m . Alternately, in analogy with Fourier transformation, $p_m(E)$ with small m has smooth E -dependence whereas $p_m(E)$ with large m will oscillate rapidly with E . Therefore, if $\langle A(E) \rangle$ varies smoothly with E over a small energy window ϵ , it will receive contributions mainly from the first few terms in (2). This will allow us to truncate (2) and make the OOPEX a viable method. The philosophy is depicted in Fig. 1. Physically, the truncation discards information that distinguishes between nearby eigenstates, but this information is stored in complicated observables that are impossible to measure in practice anyway [47].

How many terms must we retain without incurring significant truncation error? We can crudely estimate an upper bound on m_c , the value of m at which convergence occurs, as follows. Energy is extensive, $E \propto N$, while $\langle A(E) \rangle$ varies negligibly over any sub-extensive interval $\epsilon \propto N^\alpha; \alpha \rightarrow 1^-$ according to (1). Crudely assuming that the m roots of $p_m(E)$ are real and equally spaced across the spectrum, ϵ will contain a root if $m > E/\epsilon \propto N^{1-\alpha} \ll N$. Choosing $m_c \sim N^{1-\alpha} = O(1)$ as $\alpha \rightarrow 1^-$, $\langle A(E) \rangle$ will receive both positive and negative contributions from the interval ϵ for $m > m_c$. The net contribution will thus be small, signaling convergence.

This crude estimate receives two competing refinements in practice: (i) the cancellation of positive and negative contributions to $\langle A(E) \rangle$ within the window ϵ for $m > E/\epsilon$ is not exact, which means more terms must be retained in (2) to achieve convergence; and (ii) the roots

of $p_m(E)$ cluster near the middle of the spectrum, which means some cancellation occurs even when $m < E/\epsilon$, thereby decreasing m_c . In Sec. III, we find numerically for the NI Ising model that $m_c \lesssim 3 = O(1)$ indeed.

B. Compression using OFSR

So far, we have reduced the computation from diagonalization of H to repeated multiplications of H , but the runtime and storage costs are still exponential because H , written as a sparse matrix in a local basis, has at least $O(d)$ terms. To reduce these costs, we work in the OFSR [47, 48], in which operators are expressed as vectors in operator Hilbert space:

$$A = \sum_{\ell} \alpha_{\ell} \mathcal{O}_{\ell} \rightarrow ||A\rangle\rangle = (\alpha_1, \alpha_2 \dots)^T \quad (3)$$

where each \mathcal{O}_{ℓ} is a product of local operators, $\text{tr}(\mathcal{O}_{\ell}^{\dagger} \mathcal{O}_{\ell'}) = \delta_{\ell\ell'}$ and the notation $||\dots\rangle\rangle$ has been defined to denote vectors in operator Hilbert space. For instance, basis operators for an N -site lattice with spin-1/2 on each site can be taken to be $\mathcal{O}_{\ell} = 2^{-N/2} \prod_{i \in \text{sites}} \sigma_i^{\alpha}$, where σ_i^{α} is either a 2×2 identity matrix or a Pauli matrix, and \prod^{\otimes} denotes an outer product. The OFSRs of a basis operator, a local Hamiltonian and a Hamiltonian with long-range p -body interactions contain a single term, $O(N)$ terms and $O(N^p)$ terms, respectively, as opposed to $O(d)$ terms in their usual matrix representation in a local basis. As a result, the OFSR reduces storage costs from $O(d)$ to $O(N^{pm_c})$ if we truncate (2) at m_c , which is polynomial in N for $m_c = O(1)$. Naturally, the runtime is polynomial too since only polynomially large vectors are manipulated.

The OFSR is the natural language for developing the OOPEX, because each step of the algorithm, summarized in Algorithm 1, has a simple interpretation in terms of the linear algebra of the OFSR-vectors. For instance, applying standard QR -decomposition on the matrix $(||1\rangle\rangle, ||H\rangle\rangle, ||H^2\rangle\rangle, \dots)$ yields the orthonormalized Krylov space $Q = (||1\rangle\rangle, ||p_1(H)\rangle\rangle, ||p_2(H)\rangle\rangle \dots)$ as well as the coefficients $a_{km} = (R^{-1})_{km}$ and hence, the polynomials $p_m(E)$. Moreover, the trace of a product of operators reduces to the inner product of their OFSRs: $\text{tr}(B^{\dagger}A) \equiv \langle\langle B||A\rangle\rangle$, which allows computing $\langle A(E) \rangle$ easily by choosing $B = \rho(E)$. The main trade-off is that the rules for multiplying operators in their OFSRs must be derived from the non-commutative algebra of the basis operators. We find that this added cost is easily overcome by the other gains. In contrast, the OFSR is not useful for diagonalization-based algorithms such as ED because diagonalization of a matrix does not correspond to any obvious operation on its OFSR-vector.

Algorithm 1 Main steps of the OOPEX algorithm.

1. Express H as a column vector in its OFSR, $||H\rangle\rangle$.
 2. Compute the Krylov space $K = \{||1\rangle\rangle, ||H\rangle\rangle, \dots, ||H^{m_{max}}\rangle\rangle\}$ for pre-selected m_{max} via repeated multiplication with $|H\rangle$. The multiplication rules are determined by the algebra of the OFSR basis operators.
 3. Decompose K as $K = QR$ where Q is a $4^N \times (m_{max} + 1)$ orthogonal matrix and R is a $(m_{max} + 1) \times (m_{max} + 1)$ upper-triangular matrix.
 - (a) Q is precisely the orthonormalized Krylov space: $Q = (||p_0(H)\rangle\rangle, ||p_1(H)\rangle\rangle, \dots, ||p_{m_{max}}(H)\rangle\rangle)$.
 - (b) R provides $p_m(E)$ as $p_m(E) = \sum_{k=0}^m (R^{-1})_{km} E^k$.
 - (c) Using Q and $p_m(E)$, determine $||\rho(E)\rangle\rangle$ using (2).
 4. Compute the inner product $\langle\langle \rho(E)||A\rangle\rangle = \text{tr}[\rho(E)A]$.
-

C. Optimum polynomial expansion

In this section, we place the OOPEX in the broad context of polynomial expansion methods. We show that the OOPEX, unlike other methods, avoids computing the density of states. This eliminates a major source of error and is presumably responsible for rapid convergence.

Consider expressing $A(E) = \langle E|A|E \rangle$ in terms of pre-selected functions $q_m(E)$ that are orthogonal with respect to the weight $w(E)$ over an interval $E \in [-E_0, E_0]$. One can always shift and rescale the Hamiltonian H so that all the energies E_i lie in this interval. $A(E)$ can be written as

$$A(E) = \frac{w(E)}{D(E)} \sum_m \mu_m^A q_m(E) \quad (4)$$

where

$$\int_{-E_0}^{E_0} q_m(E) q_{m'}(E) w(E) dE = N_m \delta_{mm'} \quad (5)$$

and $D(E) = \sum_i \delta(E - E_i)$ is the density of states. The unknowns above are the moments μ_m^A and $D(E)$. μ_m^A are given by

$$\mu_m^A = \frac{1}{N_m} \int_{-E_0}^{E_0} A(E) q_m(E) D(E) dE = \frac{1}{N_m} \text{tr}[A q_m(H)] \quad (6)$$

The last expression is relatively easy to compute since it is simply the Hilbert-Schmidt inner product of A and $q_m(H)$, or the inner product $\langle\langle A||q_m(H)\rangle\rangle$ in terms of their OFSRs. To determine $D(E)$, one chooses $A = 1$, which gives

$$D(E) = w(E) \sum_m \mu_m^D q_m(E) \implies \mu_m^D = \frac{1}{N_m} \text{tr}[q_m(H)] \quad (7)$$

Thus, computing $A(E)$ entails separately computing the moments μ_m^A and μ_m^D , using the latter to determine $D(E)$, and finally using (4).

The OOPEX simplifies the above process by effectively choosing $w(E) = D(E)$ and $N_m = 1$. Then,

$$A(E) = \sum_m \text{tr}[Aq_m(H)]q_m(E) \quad (8)$$

where

$$\int_{-E_0}^{E_0} q_m(E)q_{m'}(E)D(E)dE = \text{tr}[q_m(H)q_{m'}(H)] = \delta_{mm'} \quad (9)$$

In other words, $q_m(E)$ defined by (9) are precisely the $p_m(E)$ defined in (2). Note that the OOPEX never explicitly calculates $D(E)$. Thus, it avoids a major source of error compared to other methods that approximate $D(E)$ and achieve faster convergence.

A well-known example of such an algorithm is the kernel polynomial method which rescales energy so that $E_0 = 1$ and uses $q_m(E) = T_m(E)/\sqrt{1-E^2}$, where $T_m(E)$ is the m^{th} Chebyshev polynomial of the first kind. $q_m(E)$ are orthonormal with respect to the weight $w(E) = \pi\sqrt{1-E^2}$ and are normalized as $N_m = (1 + \delta_{m,0})/2$. If H is an infinite dimensional random hermitian matrix, then Wigner's semicircle law states that $D(E) = \frac{2}{\pi}\sqrt{1-E^2}$, so that $w(E)/D(E) = \pi^2/2$. Then, the kernel polynomial method is equivalent to the OOPEX up to an overall factor of $\pi^2/2$ that can be absorbed into N_m . However, $D(E)$ differs significantly from the semicircle law for realistic systems with the local Hamiltonian, and accurately computing $D(E)$ can require hundreds of Chebyshev moments μ_m^D . In contrast, the OOPEX requires calculating only the moments μ_m^A since $\mu_m^D = \frac{1}{N_m}\text{tr}[q_m(H)] = \delta_{m,0}$ is trivially known.

III. ISING MODEL RESULTS

We now demonstrate the OOPEX on a prototypical NI spin model, namely, the 1D Ising model with transverse and longitudinal fields, given by

$$H = \sum_r (J\sigma_r^z\sigma_{r+1}^z + h_x\sigma_r^x + h_z\sigma_r^z) \quad (10)$$

where $\{\sigma_r^\alpha\}$ are Pauli matrices. H is integrable if any one of J , h_x and h_z vanishes, but is NI otherwise. This model is ideal for demonstrating the OOPEX because it does not harbor any non-analyticities such as phase transitions at finite temperatures. As a result, the analytic expansion in (2) is expected to converge quickly. We choose $J = 1$, $h_x = -1.05$ and $h_z = 0.5$, and open boundary conditions to prevent momentum conservation. Then, $\|H\rangle\rangle$ contains $3N - 1$ non-zero terms with N , N and $N - 1$ terms equal to h_x , h_z and J , respectively and can therefore be stored as a sparse vector of

| Operator | Index | $\ H\rangle\rangle$ | $\ H^2\rangle\rangle$ |
|------------------------|-------|---------------------|-------------------------|
| \mathbb{K} | 00 | - | $J^2 + 2h_x^2 + 2h_z^2$ |
| σ_2^x | 01 | h_x | - |
| σ_2^y | 02 | - | - |
| σ_2^z | 03 | h_z | $2Jh_z$ |
| σ_1^x | 10 | h_x | - |
| $\sigma_1^x\sigma_2^x$ | 11 | - | $2h_x^2$ |
| $\sigma_1^x\sigma_2^y$ | 12 | - | - |
| $\sigma_1^x\sigma_2^z$ | 13 | - | $2h_xh_z$ |
| σ_1^y | 20 | - | - |
| $\sigma_1^y\sigma_2^x$ | 21 | - | - |
| $\sigma_1^y\sigma_2^y$ | 22 | - | - |
| $\sigma_1^y\sigma_2^z$ | 23 | - | - |
| σ_1^z | 30 | h_z | $2Jh_z$ |
| $\sigma_1^z\sigma_2^x$ | 31 | - | $2h_xh_z$ |
| $\sigma_1^z\sigma_2^y$ | 32 | - | - |
| $\sigma_1^z\sigma_2^z$ | 33 | J | $2h_z^2$ |

Table I. OFSR of H , given by (10), and H^2 for $N = 2$. The operators are mapped to N -digit base-4 integers as $\sigma_r^0 \rightarrow 0_r$, $\sigma_r^x \rightarrow 1_r$, $\sigma_r^y \rightarrow 2_r$, $\sigma_r^z \rightarrow 3_r$, while the coefficients become the non-zero entries in a sparse vector indexed by the base-4 integers. Even though the overall length of the sparse vector grows as 4^N , the OOPEX only involves $\|H^m\rangle\rangle$ for small m , so the number of non-zero entries that need to be stored grows mildly with N as $\sim (3N)^m$.

length 4^N with only $3N - 1$ non-zero elements. Computing $\|H^m\rangle\rangle$ entails evaluating indices while keeping track of the non-commutative algebra of the Pauli operators, which is a main computational cost, but requires storing only $\sim (3N)^m$ real numbers. Table I shows the explicit OFSRs of H and H^2 for $N = 2$. All calculations were performed on a 2.7 GHz 12-core processor with 64 GB random access memory.

A. Observables

We study three simple representative observables: the 2-point function $C_{zz}(\Delta r) = \frac{1}{2(N-\Delta r)} \sum_{r,r'=r\pm\Delta r} (\langle\sigma_r^z\sigma_{r'}^z\rangle - \langle\sigma_r^z\rangle\langle\sigma_{r'}^z\rangle)$ and the 1-point functions $M_i = \frac{1}{N} \sum_r \langle\sigma_r^i\rangle$, $i = x, z$. Fig. 2 compares the expectation values of $C_{zz}(1)$, M_x and M_z using the OOPEX, ED and HTX. The match between ED and OOPEX is striking for just $m = 2$ over a wide range of energy densities $\varepsilon = E/N$, whereas HTX deviates significantly from ED even for $m = 6$ for $|\varepsilon| \gtrsim 0.5$. The inset shows rapid convergence of the OOPEX with m at both $\varepsilon_1 = -0.8475$ and $\varepsilon_2 = -0.2048$. In contrast, HTX converges poorly (well) for the former (latter) ε ; note $|\varepsilon_1| > 0.5 > |\varepsilon_2|$. Since the OOPEX and HTX are both power series-based algorithms that work best near $\varepsilon = 0$, better performance of the former is likely due to its ability to exploit the non-integrability of the system.

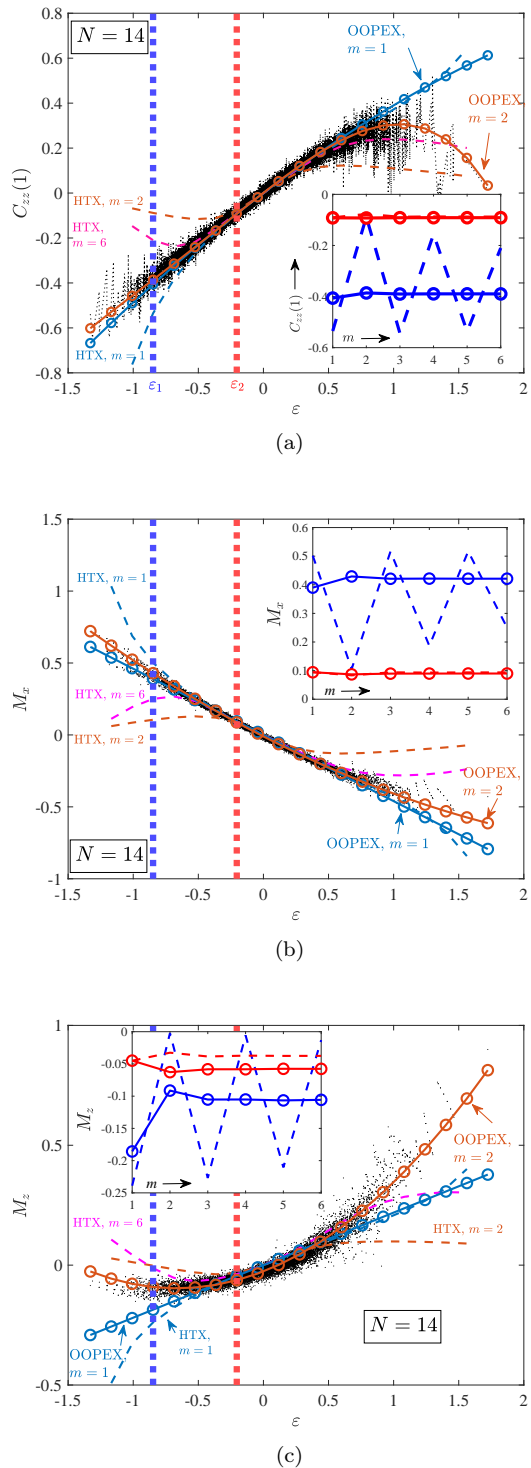


Figure 2. Comparison between computations of (a) $C_{zz}(1)$, (b) M_x and (c) M_z using OOPEX (solid with markers), ED (dotted) and HTX (dashed) for a $N = 14$ -site chain. OOPEX results for truncation at $m = 2$ agree excellently with ED whereas HTX shows significantly worse agreement even at $m = 6$. Insets show the truncation order-dependence of the OOPEX and HTX at $\epsilon_1 = -0.8475$ (blue) and $\epsilon_2 = -0.2048$ (red) marked in the main figure. The OOPEX converges almost immediately while HTX shows drastically poor convergence away from the middle of the spectrum.

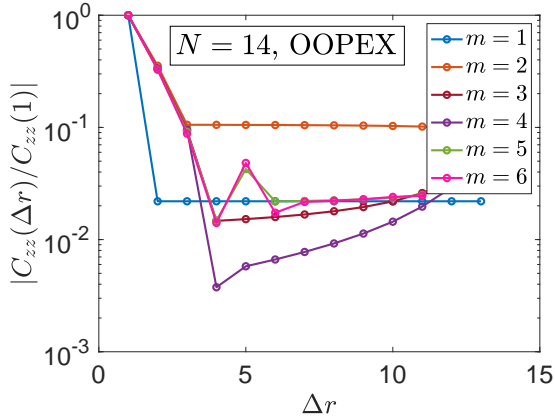
In Fig. 3, we examine the behavior of $C_{zz}(\Delta r)$ at ϵ_2 , where both HTX and OOPEX concur with ED for $C_{zz}(1)$. Figs. 3(a-c) show that access to large N with the OOPEX helps avoid finite-size effects and enables extracting a correlation length ξ . In contrast, Fig. 4 shows that extracting a correlation is unreliable using the HTX and impossible using ED at $N = 14$. At a lower energy density (relative to the ground state) ϵ_1 , HTX behaves poorly even for $C_{zz}(1)$, as Fig. 2 shows. In stark contrast, we find that the OOPEX not only works well for $C_{zz}(1)$, it works well-enough for $C_{zz}(\Delta r > 1)$ to determine ξ . Thus, we extract ξ at ϵ_1 in Fig. 5 and show that merely $m = 3$ yields ξ that is well-behaved in the thermodynamic limit. The curves flatten for large Δr because, for range- R Hamiltonians, the OOPEX can compute bare 2-point correlations between sites separated by up to $O(mR)$ sites. For larger separations, connected correlations receive contributions only from the disconnected parts. In the current example, this means $\langle \sigma_r^z \sigma_{r+\Delta r}^z \rangle = 0$ for large enough Δr so that $\langle \sigma_r^z \sigma_{r+\Delta r}^z \rangle - \langle \sigma_r^z \rangle \langle \sigma_{r+\Delta r}^z \rangle = -\langle \sigma_r^z \rangle \langle \sigma_{r+\Delta r}^z \rangle \approx \langle \sigma_r^z \rangle^2$ upto boundary effects.

B. Entanglement entropy

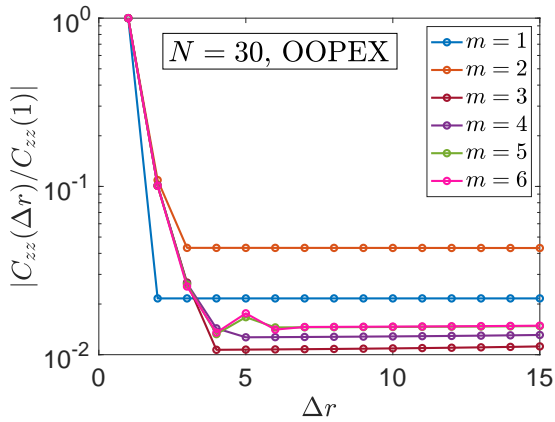
We now consider the second Renyi entanglement entropy $S_2(A)$ between the leftmost N_A sites and the rest of the system. For chaotic eigenstates, it is well-known that $S_2(A)$ follows a volume law: $S_2/N_A = O(1)$. Fig. 6 shows S_2 computed using ED, OOPEX and HTX at $\epsilon_{1,2}$ and $N = 14$. The OOPEX at $m = 3$ shows better match with ED than HTX at $m = 6$, and the linear growth with N_A is apparent. Since the OOPEX can access only short-distance correlations and $S_2(A) = \sum_{\mathcal{O}_\ell \in A} |\text{tr}(\rho \mathcal{O}_\ell)|^2$, where the sum runs over operators that have support strictly in A , the agreement between OOPEX and ED indicates that most of the Renyi entropy is carried by short-distance correlations.

Recent work argued that $S_2'' = d^2 S_2 / dN_A^2 > 0$ for chaotic eigenstates Lu and Grover [50]. Unfortunately, the hard constraints $S_2(0) = S_2(N) = 0$ and the positivity of S_2 force $S_2'' < 0$ when computed using ED at the small N it can access. However, the large N accessible with the OOPEX and the fact that the ρ produced by the OOPEX remove the constraint $S_2(N) = 0$ and enable observing $S_2'' > 0$. As shown in Fig. 7(a), $S_2'' > 0$ for almost all N_A already at $N = 14$ when $\epsilon = \epsilon_1$. When $\epsilon = \epsilon_2$, $S_2'' < 0$ for small N , but becomes > 0 when $N \gtrsim 80$. Thus, access to a large N with the OOPEX is key for detecting the convexity of S_2 .

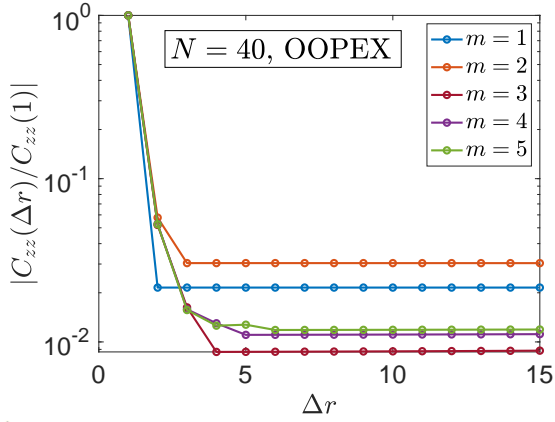
The positivity of S_2'' obtained using the OOPEX, however, must be taken with a grain of salt. Fig. 7(b) shows the m -dependence of S_2'' for several values of N at $\epsilon = \epsilon_1$. Although $S_2'' > 0$ for all the cases shown, the data clearly have not converged. However, S_2'' grows with m at larger N , suggesting that S_2'' will probably converge to a positive value. The behavior is less clear at $\epsilon = \epsilon_2$, as shown



(a)



(b)



(c)

Figure 3. Normalized $|C_{zz}(\Delta r)|$ using OOPEX at ε_2 , where HTX agrees with ED for $C_{zz}(1)$. (a) At $N = 14$, strong finite-size effects produce an upturn for $\Delta r \gtrsim 4$ that survives up to $m = 6$. (b) For $N = 30$, the upturn occurs near the opposite edge, so is missing in the data shown. Moreover, $m = 5, 6$ data nearly overlap, indicating convergence. Finally, clear exponential decay for $\Delta r \lesssim 5$ allow extracting ξ while a constant decay rate for $m = 3 \dots 6$ imply that ξ converges for $m = 3$. (c) $N = 40$ data are similar to data in (b), but the near-overlap of $m = 4, 5$ data indicate faster convergence.

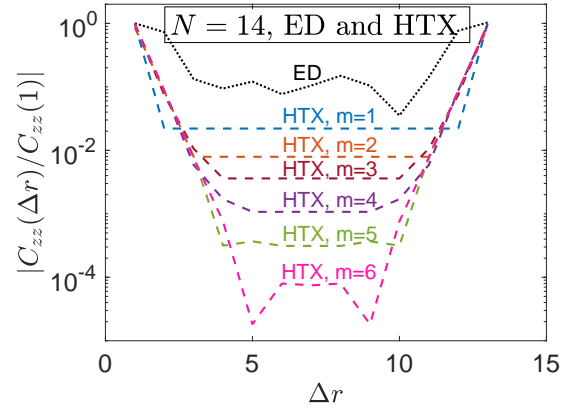


Figure 4. Normalized $|C_{zz}(\Delta r)|$ at ε_2 for $N = 14$ obtained using ED and HTX. ED data show strong finite-size effects at $N = 14$, making it impossible to determine ξ . HTX data show exponential decay for $\Delta r \lesssim 5$, but the accessible $N (\leq 14)$ is too small to perform finite-size scaling of ξ .

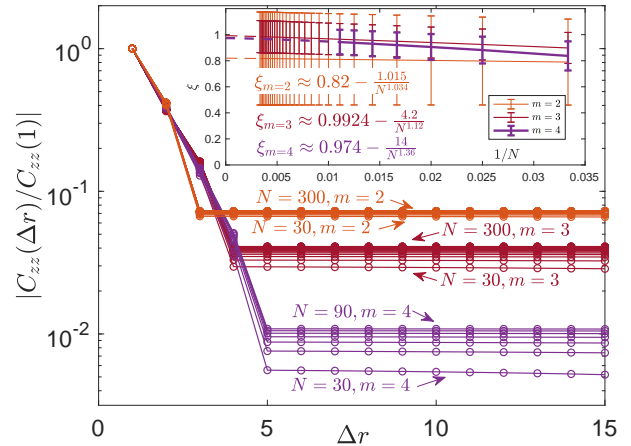


Figure 5. Normalized $|C_{zz}(\Delta r)|$ at ε_1 computed using the OOPEX for $N = 30, 40, \dots, 300$ at $m = 2, 3$ and for $N = 30, 40, \dots, 90$ at $m = 4$. Exponential decay is discernible in each data set for $1 \leq \Delta r \leq m + 1$, allowing determination of ξ . Inset shows finite-size scaling of ξ at various fixed m . For $N \rightarrow \infty$, the $m = 3, 4$ data produce nearly identical values of ξ , indicating convergence.

in Fig. 7(c). Now, S_2'' decreases with m and becomes negative for $m = 4$ for all accessible N , while increasing N at fixed m increases S_2'' . It is, thus, plausible that $S_2'' > 0$ once convergent results have been obtained in the thermodynamic limit, but our program is currently unable settle this issue.

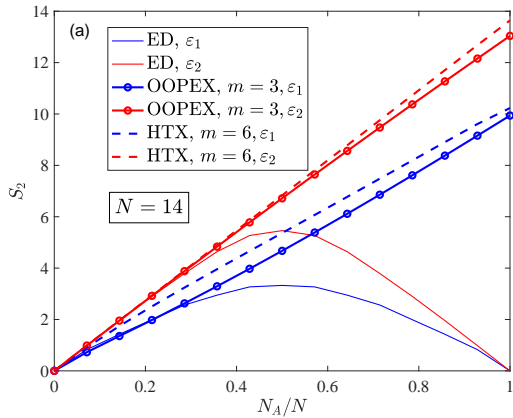


Figure 6. S_2 computed using the OOPEX, ED and HTX at $\varepsilon_{1,2}$ at $N = 14$. The OOPEX matches ED better than HTX does at a smaller truncation order.

C. Computational cost

Fig. 8 shows that time and memory needs of the OOPEX for $m = 3$ scale as power laws in N with modest exponents. In particular, the time and memory needed to create the orthonormalized Krylov space (to compute $\rho(E)$ for a fixed E given the orthonormalized Krylov space) grow as $t_{orth} \sim N^{4.1}$ ($t_\rho \sim N^{3.5}$) and $mem_{orth} \sim N^{3.95}$ ($mem_\rho \sim N^{1.86}$). Computing $\langle A(E) \rangle$ given $\rho(E)$ is practically instantaneous. However, multiplying H with itself $m - 1$ times to create the Krylov space demands resources that grow exponentially with m , which limits computations to relatively small m .

IV. CONCLUSION

In conclusion, we have introduced an algorithm, the OOPEX, that can compute expectation values in chaotic eigenstates with polynomial effort, and demonstrated it on a prototypical model. The algorithm converges rapidly thanks to the ETH, and gives access to system sizes of several hundred sites, thus enabling computations of correlation lengths that were beyond the capabilities of ED. Detailed comparisons with other algorithms including quantum Monte Carlo methods [45, 46], finite temperature density matrix renormalization group Feiguin and White [51], Jiang *et al.* [52], Karrasch *et al.* [53], Jansen *et al.* [54] and the kernel polynomial method Weiße *et al.* [49] will be presented in future work.

The OOPEX should be most useful for investigating physics in interacting regimes where ξ is finite and the E -dependence of physical quantities is smooth, such as finite temperature physics above quantum critical points and theories with a holographic gravitational dual. The fundamental reliance of the OOPEX on the ETH implies that it could be also a useful sensor of ergodicity breaking and, for example, effectively probe the many-body local-

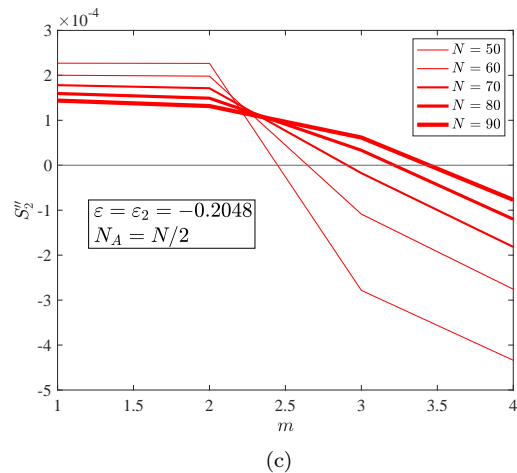
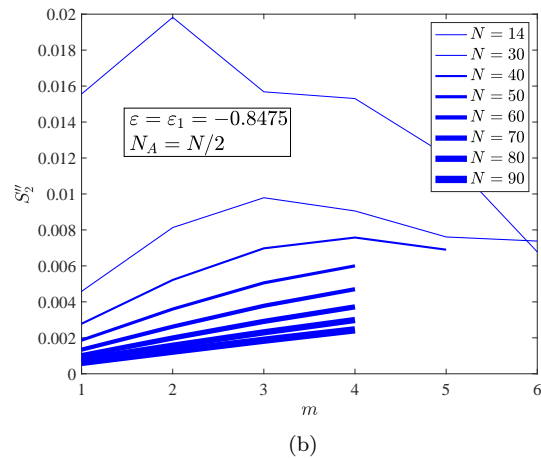
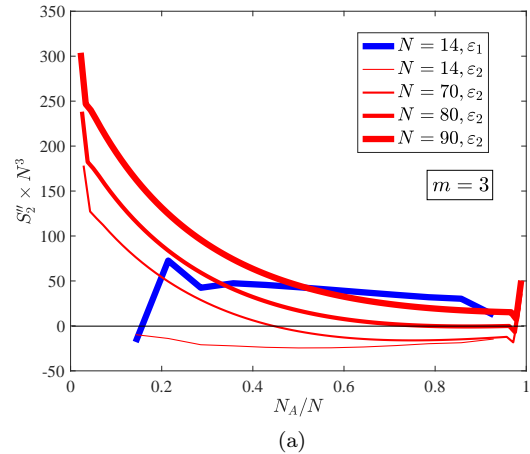
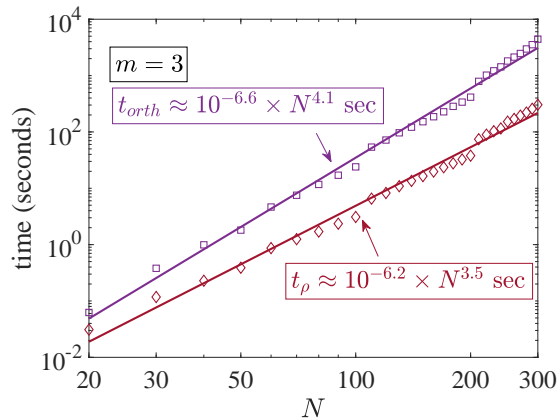
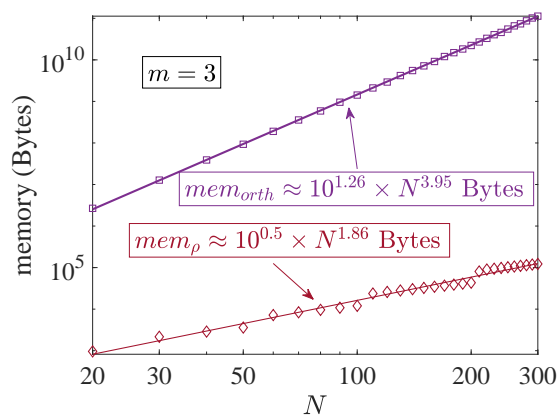


Figure 7. S_2'' computations using the OOPEX. (a) $N^3 S_2''$ vs N_A/N for $N = 14, \varepsilon = \varepsilon_1$ and various N at $\varepsilon = \varepsilon_2$. For given (m, ε) , accessing a large enough N gives a state with $S_2'' > 0$. For $(m, \varepsilon) = (3, \varepsilon_1)$, $N = 14$ suffices for almost all N_A , while $(m, \varepsilon) = (3, \varepsilon_2)$ requires $N \gtrsim 80$. The N^3 factor ensures clarity of the plot. (b) m -dependence of S_2'' at $\varepsilon = \varepsilon_1$, $N_A = N/2$ for several N . Although data does not converge, $S_2'' > 0$ always and increases with m at larger N . (c) m -dependence of S_2'' at $\varepsilon = \varepsilon_2$, $N_A = N/2$ for several N . Increasing m turns S_2'' negative, but increasing N at fixed m tends the data towards a positive S_2'' .



(a)



(b)

Figure 8. Scaling of time (a) and memory (b) requirements with N at fixed $m = 3$. t_{orth} (t_ρ) denotes the time required to compute the orthonormalized Krylov space (compute $\rho(E)$ at fixed E given the orthonormalized Krylov space), while mem_{orth} (mem_ρ) denotes the minimum memory needed to compute this space (to store $\rho(E)$ at fixed E).

ization transition from the chaotic side. Finally, while extracting critical exponents associated with phase transitions may be challenging for the OOPEX, it might help identify the *presence* of a phase transition via a broad peak in the E -dependent correlations of the order parameter. These problems will be investigated in the future.

ACKNOWLEDGMENTS

We acknowledge invaluable discussions with Xiaoliang Qi, Ashvin Vishwanath, Scott Aaronson and especially Hitesh Changlani and Fabien Alet. We acknowledge support from the Division of Research, Department of Physics and the College of Natural Sciences and Mathematics at the University of Houston and from NSF-DMR-2047193.

-
- [1] S. A. Parameswaran and R. Vasseur, Reports on Progress in Physics **81**, 082501 (2018).
[2] R. Nandkishore and D. A. Huse, Annual Review of Condensed Matter Physics **6**, 15 (2015).
[3] A. Pal and D. A. Huse, Phys. Rev. B **82**, 174411 (2010).
[4] F. Alet and N. Laflorencie, Comptes Rendus Physique, <https://doi.org/10.1016/j.crhy.2018.03.003> (2018).
[5] H. Bethe, Zeitschrift für Physik **71**, 205 (1931).
[6] E. Gutkin, Annals of Physics **176**, 22 (1987).
[7] J. Y. Lee, X. W. Guan, A. del Campo, and M. T. Batchelor, Phys. Rev. A **85**, 13629 (2012).
[8] B. Sutherland, Phys. Rev. Lett. **75**, 1248 (1995).
[9] K. R. Fratus and M. Srednicki, Phys. Rev. E **92**, 040103 (2015).
[10] K. R. Fratus and M. Srednicki, arXiv e-prints, arXiv:1611.03992 (2016).
[11] F. Pastawski, B. Yoshida, D. Harlow, and J. Preskill, JHEP **06**, 149 (2015), arXiv:1503.06237 [hep-th].
[12] A. Almheiri, X. Dong, and D. Harlow, JHEP **04**, 163 (2015), arXiv:1411.7041 [hep-th].
[13] F. G. S. L. Brandão, E. Crosson, M. B. Şahinoğlu, and J. Bowen, Phys. Rev. Lett. **123**, 110502 (2019).
[14] N. Bao and N. Cheng, Journal of High Energy Physics **2019**, 152 (2019).
[15] J. R. Garrison and T. Grover, Phys. Rev. X **8**, 021026 (2018).
[16] X.-L. Qi and D. Ranard, Quantum **3**, 159 (2019).
[17] N. Lashkari, A. Dymarsky, and H. Liu, Journal of High Energy Physics **2018**, 70 (2018).
[18] Y. Hikida, Y. Kusuki, and T. Takayanagi, Phys. Rev. D **98**, 026003 (2018).
[19] S. Datta, P. Kraus, and B. Michel, Journal of High Energy Physics **2019**, 143 (2019).
[20] N. Lashkari, A. Dymarsky, and H. Liu,

- Journal of Statistical Mechanics: Theory and Experiment , 033101 (2018), 12.5123 [hep-th].
- [21] J. Maldacena, International Journal of Theoretical Physics **38**, 1113 (1999).
- [22] X.-L. Qi, eprint arXiv:hep-th/1309.6282 (2013), arXiv:1309.6282 [hep-th].
- [23] S. Popescu, A. J. Short, and A. Winter, Nat Phys **2**, 754 (2006).
- [24] N. Linden, S. Popescu, A. J. Short, and A. Winter, Phys. Rev. E **79**, 61103 (2009).
- [25] J. M. Deutsch, Phys. Rev. A **43**, 2046 (1991).
- [26] J. M. Deutsch, New Journal of Physics **12**, 75021 (2010).
- [27] J. v. Neumann, Zeitschrift für Physik **57**, 30 (1929).
- [28] A. O. Lopes and M. Sebastiani, e-prints: quant-ph:1507.02736 (2015), arXiv:1507.02736 [quant-ph].
- [29] J. von Neumann, The European Physical Journal H **35**, 201 (2010).
- [30] L. D'Alessio, Y. Kafri, A. Polkovnikov, and M. Rigol, Advances in Physics **65**, 239 (2016), <https://doi.org/10.1080/00018732.2016.1198134>.
- [31] P. Reimann, Phys. Rev. Lett. **99**, 160404 (2007).
- [32] P. Reimann, New Journal of Physics **17**, 55025 (2015).
- [33] M. Srednicki, Phys. Rev. E **50**, 888 (1994).
- [34] M. Srednicki and F. Stiernelof, Journal of Physics A: Mathematical and General **29**, 5817 (1996).
- [35] M. Srednicki, Journal of Physics A: Mathematical and General **32**, 1163R (1999).
- [36] J. Maldacena and D. Stanford, Phys. Rev. D **94**, 106002 (2016).
- [37] J. Polchinski and V. Rosenhaus, Journal of High Energy Physics **2016**, 1 (2016).
- [38] D. A. Roberts and B. Swingle, Phys. Rev. Lett. **117**, 91602 (2016).
- [39] D. A. Roberts and D. Stanford, Phys. Rev. Lett. **115**, 131603 (2015),
- [40] S. H. Shenker and D. Stanford, Journal of High Energy Physics **2014**, 67 (2014).
- [41] S. Xu, X. Li, Y.-T. Hsu, B. Swingle, and S. Das Sarma, Phys. Rev. Research **1**, 032039 (2019).
- [42] L. Foini and J. Kurchan, Phys. Rev. E **99**, 042139 (2019).
- [43] J. Maldacena, S. H. Shenker, and D. Stanford, Journal of High Energy Physics **2016**, 106 (2016), arXiv:1503.01409 [hep-th].
- [44] P. Hosur, X.-L. Qi, D. A. Roberts, and B. Yoshida, Journal of High Energy Physics **2016**, 4 (2016).
- [45] M. Troyer and U.-J. Wiese, Phys. Rev. Lett. **94**, 170201 (2005).
- [46] Y. Loh, J. E. Gubernatis, R. T. Scalettar, S. R. White, D. J. Scalapino, and R. L. Sugar, Phys. Rev. B **41**, 9301 (1990).
- [47] P. Hosur and X.-L. Qi, Phys. Rev. E **93**, 42138 (2016).
- [48] V. Ros, M. Mueller, and A. Scardicchio, Nuclear Physics B **891**, 420 (2015).
- [49] A. Weiße, G. Wellein, A. Alvermann, and H. Fehske, Rev. Mod. Phys. **78**, 275 (2006).
- [50] T.-C. Lu and T. Grover, Phys. Rev. X **9**, 032111 (2019).
- [51] A. E. Feiguin and S. R. White, Phys. Rev. B **72**, 220401 (2005).
- [52] T. Jiang, W. Li, J. Ren, and Z. Shuai, *The Journal of Physical Chemistry Letters*, The Journal of Physical Chemistry Letters **11**, 3761 (2020).
- [53] C. Karrasch, J. H. Bardarson, and J. E. Moore, New Journal of Physics **15**, 083031 (2013).
- [54] D. Jansen, J. Boncca, and d. F. Heidrich-Meisner, Phys. Rev. B **102**, 165155 (2020).